12th International Symposium on Turbulence and Shear Flow Phenomena (TSFP12)
Osaka, Japan (Online), July 19-22, 2022

ON THE STABILITY AND TRANSITION TO TURBULENCE OF THE FLOW OVER A WIND-TURBINE AIRFOIL UNDER VARYING FREE-STREAM TURBULENCE INTENSITY

Thales C. L. Fava[1]
fava@kth.se

Brandon A. Lobo[2]
brandon.a.lobo@fh-kiel.de

Alois P. Schaffarczyk[2]
alois.schaffarczyk@fh-kiel.de

Michael Breuer[3]
breuer@hsu-hh.de

Ardeshir Hanifi[1]
hanifi@kth.se

Dan Henningson[1]
henning@mech.kth.se

[1]Department of Engineering Mechanics, KTH Royal Institute of Technology, SE-100 44 Stockholm, Sweden
[2]Mechanical Engineering Department, Kiel University of Applied Sciences, D-24149 Kiel, Germany
[3]Department of Fluid Mechanics, Helmut-Schmidt-University Hamburg, D-22043 Hamburg, Germany

ABSTRACT

The present work investigates the laminar-turbulent transition of the flow around a typical section of a wind turbine blade under different levels of isotropic inflow turbulence at a Reynolds number of $Re_c = 10^5$. Wall-resolved large-eddy simulations are performed under different turbulence intensities (TI) up to $TI = 2.8$ %. The results are analyzed with tools based on the linear stability and optimal-perturbation theory. At $TI = 0\%$, transition to turbulence via the breakdown of Kelvin-Helmholtz (KH) rolls formed over the laminar separation bubble (LSB) is seen. These modes start to grow upstream of the LSB as an inflectional instability. At $TI = 1.4$ % rolls are also seen; but, instabilities formed by the interaction between streaks and the LSB also contribute to transition. The streaks are estimated to have a spanwise wavenumber around $\beta = 100$ ($\beta\delta^* = 0.19$ at 20 % chord; δ^* is the displacement thickness) and a frequency in the range $f = 5-8$ ($f\delta^*/u_e = (1.4-2.3)\times 10^{-2}$ at 40 % chord; u_e is the boundary layer edge velocity), close to that of the shear-layer instability. In the $TI = 2.8$ % case, the flow is heavily influenced by the presence of streaks, which stabilize the flow concerning inflectional/KH instabilities, but, at the same time, undergoes varicose-type instabilities and breakdown to turbulence.

INTRODUCTION AND METHODOLOGY

For the design of wind turbine blades with increased energy output and lifespan and reduced noise emissions, it is paramount that the transition mechanisms under free-stream turbulence (FST) with varying turbulence intensities (TI) and length scales are better understood. Different transition scenarios are known to occur within the boundary layer depending on the scale and intensity of the FST. For low TI, typically $TI < 0.5-1$ %, transition usually takes place through two-dimensional Tollmien-Schlichting (TS) instabilities (Reshotko, 1976). The TS instability may arise in flows with no pressure gradient through a viscous mechanism. In the presence of an adverse pressure gradient, the velocity profiles may become inflectional, allowing an inviscid instability.

At higher TI, bypass transition occurs. This refers to transition processes with an initial growth not described by the exponential amplification of the main modes of the Orr-Sommerfeld/Squire equations. This often results in streamwise-elongated structures called streaks, regions of high or low streamwise velocity compared to the mean flow. Both sinusoidal and varicose modes have been identified, and their mechanism is well documented (Asai *et al.*, 2002).

Recent measurements on a wind turbine (Schaffarczyk *et al.*, 2017) in the free atmosphere found that transition via TS instabilities was unlikely and that Mack's correlation (from wind tunnel studies) for the amplification factor was not directly applicable. Özçakmak *et al.* (2020) showed experimentally and numerically that bypass transition occurs under high FST, while natural transition by TS waves happens otherwise.

The present work aims at identifying and characterizing the flow instabilities triggering transition over a section of a wind turbine blade of the type LM45.3p (20 % thickness) in the presence of inflow turbulence at varying TI. This analysis is done using wall-resolved large-eddy simulations (LES) and linear stability analysis. Three test cases are considered with $TI = 0,\ 1.4,$ and 2.8 %. Turbulence is generated with the synthetic turbulence inflow generator proposed by Klein *et al.* (2003) and injected within the domain (Breuer, 2018). Isotropic turbulence is generated with an integral length scale $L/c = 0.118$ and a time scale $T = L/u_\infty$ extracted from the experimental work of Hain *et al.* (2009) and also used by Breuer (2018). All cases have a constant angle of attack of 4° and a chord Reynolds number $Re_c = u_\infty c/\nu = 10^5$. The generation and injection of the inflow turbulence into the LES domain and corresponding results and conclusions are found in Lobo *et al.* (2022). All units are non-dimensionalized by the inflow velocity (u_∞) and chord length (c).

RESULTS
Flow Characterization

Table 1 summarizes certain parameters of the different flow cases such as the locations of the leading and trailing edges of the laminar separation bubble (LSB) (x_{b_1} and x_{b_2}), the location and the value of the LSB maximum height ($x_{y_{\max}}$ and

$y_{\max}/\delta^*$, δ^* being the local displacement thickness). Also included are the positions downstream of which adverse pressure gradient (APG) and inflectional velocity profiles occur (x_a and x_i). The start of transition is given by the x location where the Reynolds stresses normalized by the free-stream velocity reach the threshold $-\overline{u'v'}/u_\infty^2 = 0.001$ (x_{tr_1}) (Yuan *et al.*, 2005).

Table 1: Characteristics of the LSB and transition.

TI	x_{b_1}	x_{b_2}	$x_{y_{max}}$	y_{max}/δ^*	x_a	x_i	x_{tr_1}
0.0 %	0.50	0.74	0.62	0.51	0.33	0.38	0.50
1.4 %	0.51	0.76	0.64	0.48	0.34	0.34	0.44
2.8 %	0.52	0.75	0.63	0.38	0.34	0.39	0.39

As indicated in Table 1, at a TI of 0 %, a LSB is formed in the region $x = 0.50 - 0.74$, with a maximum height of $0.51\,\delta^*$ at $x = 0.62$, as a result of the adverse pressure gradient (APG) that acts for $x > 0.33$. With an increase in TI to 1.4 %, the LSB is slightly displaced downstream with its height reduced to $0.48\,\delta^*$, which is connected to the entrainment of fluid into the LSB by the vortices formed close to its trailing edge (Burgmann & Schröder, 2008) and to the enhancement in the near-wall momentum by the non-linear interaction between streaks and streamwise vortices (Karp & Hack, 2020). However, the amplitude of the streaks is not high enough to trigger bypass transition. Moreover, the beginning of amplification moves 6 % upstream to $x_{tr_1} = 0.44$ A further increase in TI to 2.8 % promotes an additional reduction in the size of the LSB, with its maximum height dropping to $0.38\,\delta^*$ (25 % reduction compared to $TI = 0$ %). Furthermore, transition starts earlier ($x_{tr_1} = 0.39$), which coincides with x_i, indicating that the growth is likely due to an inflectional instability.

To gain insight into the structures responsible for transition, the contours of streamwise velocity perturbations (u') on the suction side are plotted in Fig. 1 for arbitrary snapshots. Considering the $TI = 0$ % case shown in Fig. 1a, the formation of spanwise-uniform wavefronts (spanwise wavenumber $\beta = 0$) is seen starting at $x = 0.38$, which is the same location where the flow becomes inflectional. Therefore, they are possibly related to an inflectional instability. These structures agree with Squire's theorem stating that two-dimensional disturbances are the first to become unstable in a parallel flow, which is observed despite the non-parallelism of the current flow. The presence of an inflection point for $x \geq 0.38$ also fulfills Rayleigh's necessary condition for shear-flow instability. The frequency of these waves can be estimated from the temporal auto-correlation of the normal velocity perturbations (R_{vv}) for a point inside the boundary layer by defining the period of these waves as half the distance to the first minimum of R_{vv}. Figure 2a shows a plot of these frequencies along the chord. It is possible to infer that the frequency of the dominant flow structures upstream of the LSB ($x = 0.4$ and 0.5), which are spanwise wavefronts, is $f = 9.6$. Furthermore, a sharp rise is noticed already at $x = 0.25$, i.e., before the appearance of the inflection point and the corresponding spanwise rolls at $x = 0.38$. Stability analyses with the Orr-Sommerfeld and parabolized stability equations (PSE) showed no unstable mode upstream of the inflection point, ruling out viscous instabilities as the cause of this rise in frequency. However, the elliptical nature of the pressure equation allows disturbances to be felt upstream, which may be the reason behind the increase in amplitude for frequencies that are stable upstream of the inflectional region. Additionally, spanwise rolls appear at

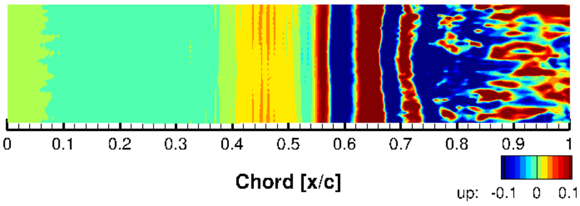

(a) $TI = 0$ %

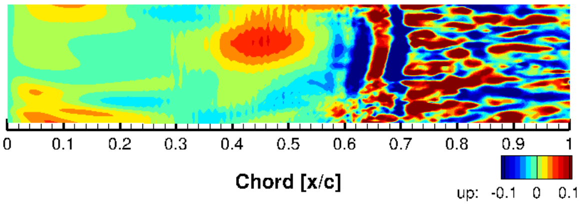

(b) $TI = 1.4$ %

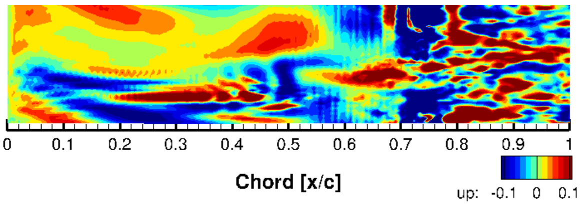

(c) $TI = 2.8$ %

Figure 1: Contours of streamwise velocity perturbations (u') (arbitrary snapshot ($T = 9.4$)). Slices are taken at a wall-normal height equal to the displacement thickness at 20 % chord.

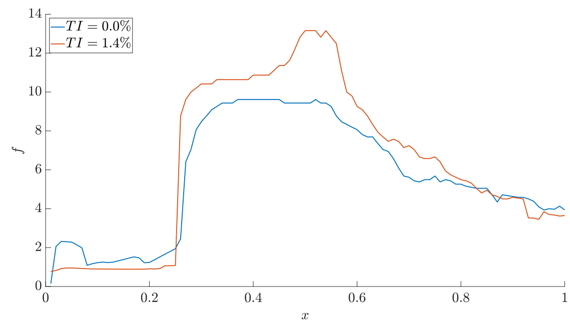

(a) Frequency (f) for $TI = 0$ % and $TI = 1.4$ %.

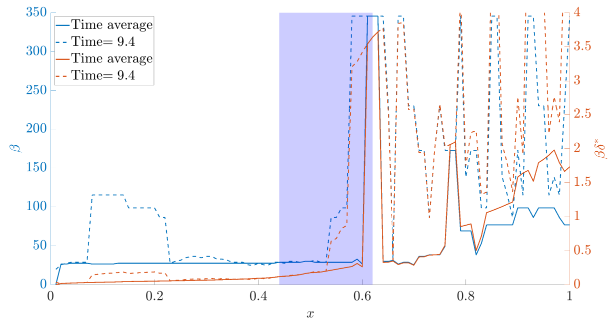

(b) Spanwise wavenumber (β) scaled by the chord and displacement thickness ($\beta\delta^*$) for $TI = 1.4$ %. Blue area shows transition.

Figure 2: Frequency and spanwise wavenumber from auto-correlations of normal and streamwise velocity perturbations, respectively, at $y = 0.5\delta^*$.

$x = 0.54$, with higher amplitude and larger streamwise wavelength than the modes growing upstream of separation. It is worth noting that these structures appear shortly after the inception of the LSB, and they have been attributed to the roll-up of the shear layer due to a KH instability as noticed in numerical (Jones *et al.*, 2010) and experimental studies (Burgmann & Schröder, 2008). The frequency of these rolls can be estimated as seen in Fig. 2a, which yields $f = 7.8$ for $x = 0.6$, slightly lower than the frequency of the waves upstream of the separation bubble. The KH rolls begin to break down around 70 % chord. Reattachment at $x = 0.74$ promotes fully turbulent flow.

Similar structures as those observed in the case with no inflow turbulence are also identified for the $TI = 1.4$ % case (see Fig. 1b). Spanwise-uniform wavefronts are observed at $x = 0.34$, which matches the position where the APG and, correspondingly, the inflection starts to act. The frequency of these waves is estimated from R_{vv} presented in Fig. 2a that yields $f = 10.4$, 10.9, and 13.2 for $x = 0.3$, 0.4, and 0.5, respectively. The increase in frequency seen at $x = 0.5$ coincides with the location where streaks interact with the separated shear layer. It is known that streaks faster than the mean flow interact with the instantaneous separation bubble and shift separation downstream, whereas streaks slower than the mean flow shift the separation bubble upstream (Lobo *et al.*, 2022). A corresponding rise in frequency is also found in the amplitude spectrum discussed later. Larger 2D rolls of the KH kind are observed as early as $x = 0.52$ (time-dependent). This is immediately downstream of the leading edge of the separation bubble located at $x = 0.51$. The frequency of these rolls can be estimated as $f = 9.3$ at $x = 0.6$ and $f = 7.7$ at $x = 0.65$, a similar frequency as in the case with $TI = 0$ %. The spanwise wavenumber (β) of the streaks, which are seen to originate near the leading edge of the airfoil, can be estimated from the spatial auto-correlation in the spanwise direction of the streamwise velocity perturbations inside the boundary layer (R_{uu}). The results are displayed in Fig. 2b, which shows the time-averaged and instantaneous values of β and $\beta\delta^*$. The time-averaged value β tends to remain constant close to $\beta = 25$ (corresponding to waves spanning the whole span) until it displays a sharp rise at the x-position of the breakdown of the KH rolls, probably due to the generation of structures with smaller wavelengths. However, the instantaneous β–distribution indicates the presence of structures with $\beta = 115.2$ at $x = 0.10$ and $\beta = 98.7$ at $x = 0.15$ and 0.20, which correspond to the streaks seen in Fig. 1b. Their absence in the time-averaged β–distribution may be linked to a temporal scarcity of these structures at relatively low TI levels.

The results for the $TI = 2.8$ % case are presented in Fig. 1c. Streaks that start to develop close to the leading edge of the airfoil seem to dominate the flow over the spanwise-uniform disturbances associated with modal growth. However, it is still possible to observe reminiscences of the 2D wavefronts and rolls in the region $x = 0.55 - 0.62$, which is inside the LSB. Unfortunately, data were collected only at specific flow locations for this case, preventing the inclusion of auto-correlation analyses in time and spanwise direction.

Flow Stability and Transition

The amplitude spectral density of the streamwise velocity perturbations at nine locations along the chord are presented in Fig. 3. For $TI = 0$ % (Fig. 3a), there is a significant increase in the perturbation amplitude at $x = 0.3$ ($Re_{\delta^*} = 193$) to $x = 0.5$ ($Re_{\delta^*} = 435$) in the range $f = 3.6 - 20.0$, with a maximum around $f = 7.8$ at $x = 0.4$ and 0.5. The fact that the frequency increases with x in the current case until $x = 0.5$ is possibly

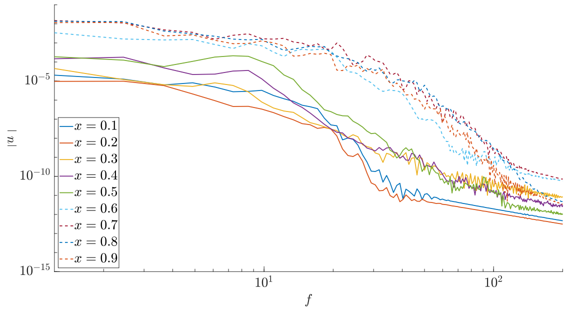

(a) $TI = 0$ %

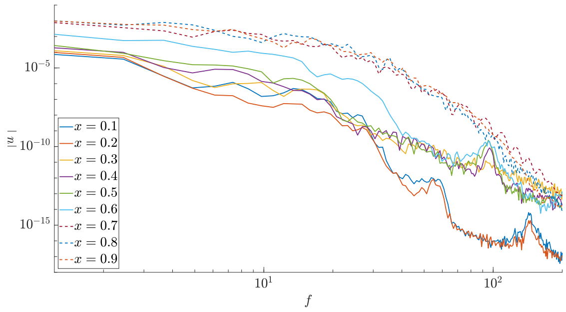

(b) $TI = 1.4$ %

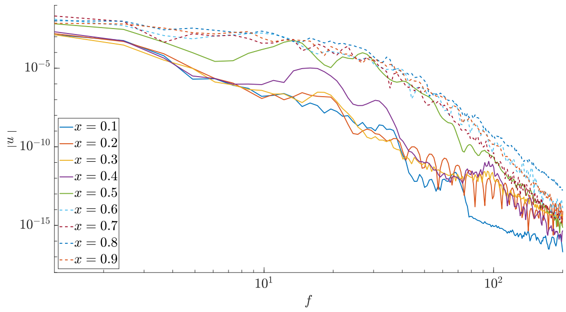

(c) $TI = 2.8$ %

Figure 3: Amplitude spectral density of streamwise velocity perturbations. Dashed lines indicate that the station presents turbulent regions.

related to a strong APG. The 2D waves evolving upstream of the LSB present $\lambda_x = 5.5 \times 10^{-3}$ at $x = 0.46$ (spanwise roll seen in Fig. 1a) and $f = 9.6$ (see Fig. 2a), which lies within the range observed in the PSD and yields a phase speed $c_s = 0.053$ while the RMS of the fluctuating streamwise velocity component at this location has a speed $u_{rms} = 0.049$ This phase speed is lower than that of TS waves, generally found in the interval $c_s = 0.3 - 0.4$. Once again, a growth is noticed in the PSD at $x = 0.3$ occurring in the same range of frequencies observed at $x = 0.4$ and 0.5. This is attributed to the elliptical nature of the pressure equation. The phase speed of the rolls in the separated shear layer can also be estimated from $\lambda_x = 0.05$ retrieved from Fig. 1a and $f = 7.8$ (Fig. 2a), which gives $c_s = 0.40$. This is in the range reported by Dovgal *et al.* (1994) and Yarusevych *et al.* (2008) for KH instabilities developing over an LSB on an airfoil. Thus, it is possible to associate the rolls evolving over the LSB to the shear layer roll-up due to a KH instability. The spectrum for $x \geq 0.6$ presents a broadband characteristics typical for turbulent flow.

The spectrum of the $TI = 1.4$ % (Fig. 3b) reveals an amplitude rise in the range $f = 3.6 - 20.0$ for $x = 0.4$ and 0.5. Moreover, the wavefronts evolving upstream of the LSB at $x = 0.3$ to 0.5 have frequencies of $f = 10.4 - 13.2$ (Fig. 2a),

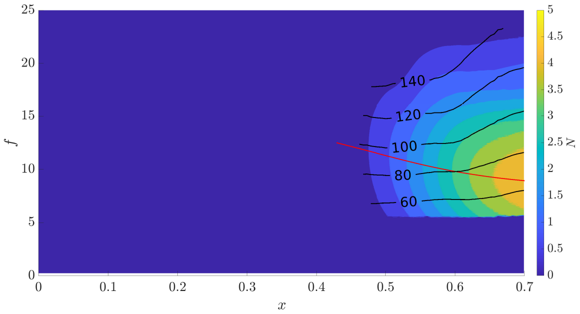

(a) $TI = 0$ %.

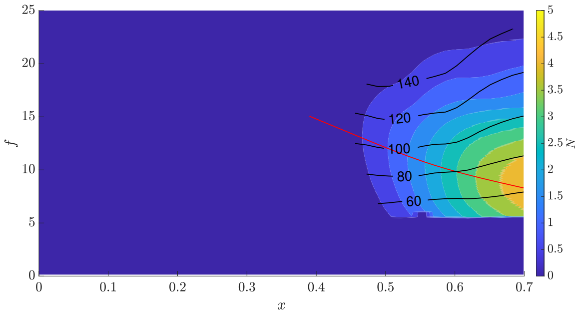

(b) $TI = 1.4$ %.

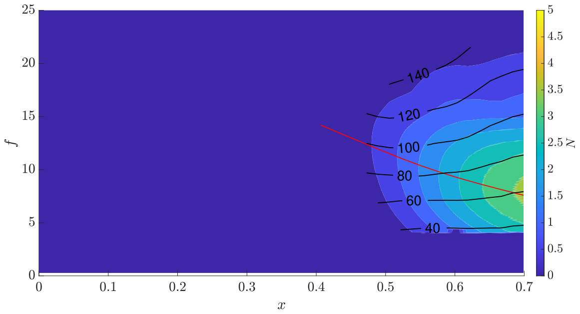

(c) $TI = 2.8$ %.

Figure 4: Contours of N factor from PSE analysis for $\beta = 0$. The black lines are isolines of the real part of the streamwise wavenumber α, and the red line represents the coordinates of the maximum N factor.

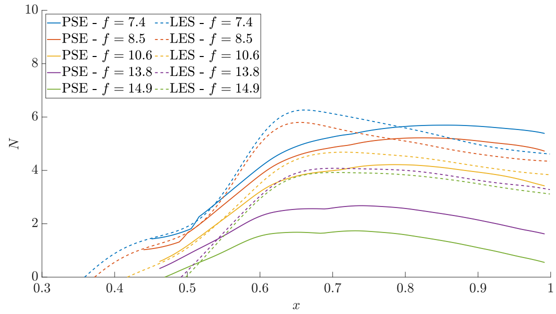

(a) $TI = 0$ %.

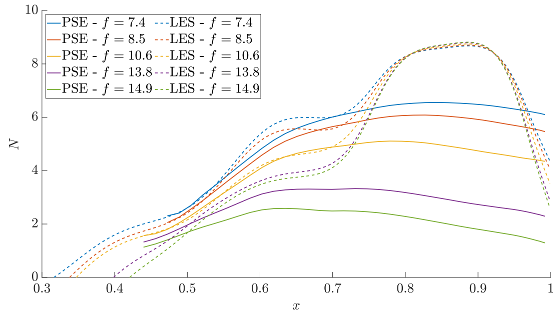

(b) $TI = 1.4$ %.

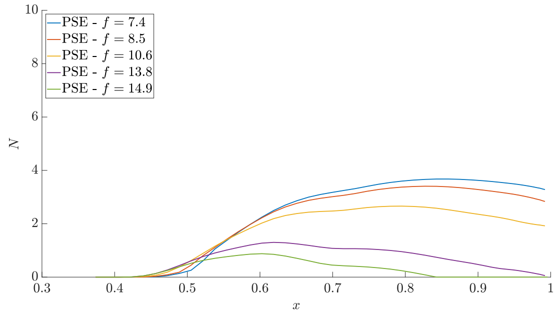

(c) $TI = 2.8$ %.

Figure 5: N factor versus x of the modes constituting the envelope of amplification for $\beta = 0$.

with a corresponding amplitude growth in the spectrum. This is particularly visible at $x = 0.5$, with the first region of high amplitude around $f = 7.8$ and the second around $f = 13.2$. The KH rolls are associated with $f = 7.8$ as discussed for the case with $TI = 0$ %. However, $x = 0.5$ is upstream of the location of the separation bubble and this upstream peak is once again attributed to the elliptical nature of the pressure equation. As discussed earlier, the peak at $f = 13.2$ corresponds to the interaction of the streaks with the separation bubble.

The results for $TI = 2.8$ %, displayed in Fig. 3c, indicate an amplitude growth in the range $f = 12 - 24$ for $x = 0.2$ and 0.3. This is the location where the overlap of a high- and low-speed streak first takes place (see Fig. 1c) and is described in detail in Lobo *et al.* (2022). This seems to possess a similar frequency as that described earlier for $TI = 1.4$ % on the interaction of high-speed streaks and the separation region (negative mean velocity). It is possible that these interactions, which are both an overlap of a relatively high-velocity region with that of a low-velocity region (compared to the mean flow), possess a similar frequency. At $x = 0.4$, an increase in amplitude can be seen in the range $f = 7.3 - 47.6$, with a significant amplification around $f = 15.8$ and 30.5. This is too high for the growth of streaks, as discussed later in the optimal-perturbation analysis, but it corresponds to the location of the appearance of the varicose mode that is formed by the interaction of the high and low-speed streaks. These frequencies are in the range of those indicated by Asai *et al.* (2002) (after a proper nondimensionalization) for varicose modes on a flat plate. Moreover, flow visualizations indicate the presence of a varicose mode at $x = 0.4$, where it is possible to see the breakdown of a streak in Fig. 1c. Snapshots showing this instability in more detail can be found in Lobo *et al.* (2022).

To identify the modes responsible for the flow instability, PSE analysis is used to compute the evolution of the N factor with x as a function of f. Only $\beta = 0$ modes were considered, as they are the most unstable ones for parallel shear flows, and the structures observed in the simulations at $TI = 0$ % are spanwise-uniform. Notice that streaks cannot be computed with the PSE as they have the streamwise wavenumber (α) equal to zero. The results are shown in Fig. 4, where the black lines are isocontours of α. For $TI = 0$ % (Fig. 4a), the unstable region spans the range $f = 5.4 - 21.1$ and the maximum amplification occurs around $f = 12.6$, 11.3, and 9.8 for $x = 0.4$, 0.5, and 0.6, respectively. However, the maximum amplification tends to the frequency $f = 7.8$ as x increases, the same

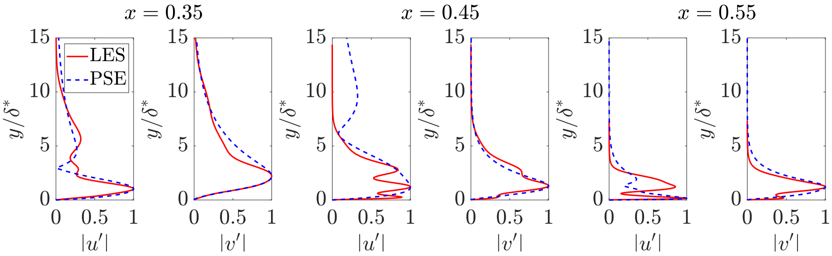

Figure 6: Normal profiles of the absolute value of streamwise (u') and normal (v') velocity perturbations for $f = 7.4$ and $\beta = 0$. The wall-normal coordinate is normalized by the local displacement thickness.

frequency obtained from the PSD for $x = 0.4$ and 0.5. This further indicates that the peaks observed in the spectrum at $f = 7.8$ for $x = 0.4$ and 0.5 result from a propagation of these disturbances as discussed earlier and, therefore, cannot be predicted in the PSE computations.. There is also a drop in α (rise in λ_x), observed in the inflectional and KH instabilities as they evolve in x. Figure 4b shows the results for $TI = 1.4\%$. The instability region is quite similar to that of the $TI = 0$ % case, but it displays slightly lower growth rates. This could be on account of the streaks, as discussed earlier. Besides, a more accentuated drop in f and α of the most amplified wave, i.e., the inflectional instabilities developing upstream of the LSB, present higher f and α, whereas the KH instability in the LSB presents lower values of these parameters compared to the $TI = 0$ % case. The highest growth occurs at $f = 7.8$ as x increases, which agrees with the frequency of the amplitude peak in the PSD for $x = 0.4$ and 0.5. . For a further increase in the turbulence intensity to $TI = 2.8$ %, as shown in Fig. 4c, the N factor is substantially reduced due to the mean-flow distortion promoted by streaks, particularly the transport of momentum to the near-wall region and reduction of the size of the LSB. The maximum amplification takes place at $f = 7.2$, and the value of α for maximum amplification also decreases in relation to the lower TI cases. This issue indicates that modal instabilities with longer wavelengths are more amplified under higher TI values. Moreover, no particular amplitude rise at this frequency could be noticed in the spectrum, which shows that the main instability mechanism changes from modal to non-modal from $TI = 1.4$ % to 2.8 %.

Figure 5 shows the N factor from the PSE and LES (after FFT) as a function of x of the modes that constitute the envelope of amplification. Since the PSE is a linear method, one can move its N-factor curves in the vertical direction. This is done to match the slopes of the LES results, which represent the amplification rates. For the $TI = 0$ % case, the first mode to start amplification is at $f = 7.4$, which occurs upstream of the region of inflection. However, the PSE analysis does not predict any unstable mode in this region, which is expected based on our earlier discussions regarding the origin of these modes at upstream locations. Moreover, for $f = 7.4$ and 8.5 the slope of the N factor curves becomes steeper around $x = 0.5$, where the LSB is formed, indicating higher amplification in the separated region compared with the area with inflectional velocity profiles upstream of the bubble ($x = 0.38 - 0.50$). The amplification downstream of separation agrees with the analysis that this mode is associated with the KH instability. Close agreement between the amplification rates of the PSE and LES is obtained for $f = 7.4$, 8.5, and 10.6 in the range $x = 0.45 - 0.56$, particularly for the latter frequency. Further downstream, the agreement reduces because the amplitude of the rolls is high enough to trigger non-linear effects. The modes with $f = 13.8$ and 14.9, obtained from the PSE, display lower growth rates than those from the LES, which could not be explained so far.

Considering the $TI = 1.4$ % case, the $f = 7.4$ mode is again the first one to present a rise in amplitude upstream of the region with inflectional velocity profiles. However, unlike the $TI = 0$ % case, there is further amplification after a local maximum inside the separation bubble at $x = 0.66$, where the KH rolls start to break down. If only the region $x \leq 0.66$ is considered, one notices that the modes display a lower amplification compared to the $TI = 0$ % case, which indicates that the streaks and disturbances entering the boundary layer dampen the inflectional and KH instabilities, probably by reducing the inflectional character of the flow and the LSB, as shown in Table 1. An even better agreement between the growth rates from PSE and LSE is obtained for this case. This is particularly true for the $f = 10.6$ mode, but also for the $f = 7.4$ and 8.5 ones. Finally, the $TI = 2.8$ % case, for which only PSE results are available, indicates that the frequency of $f = 7.4$ still displays the maximum growth and growth rate. Nevertheless, due to the increase of momentum mixing close to the wall by the incoming perturbations and streaks, which renders the flow less unstable, the growth displayed for this case is lower.

Figure 6 displays the shape of the absolute value of streamwise (u') and normal (v') velocity perturbations from LES (after FFT) and PSE for $TI = 0$ %. Only a mode close to the most amplified frequency is shown. At $x = 0.35$, i.e., upstream of the region of inflectional velocity profiles ($x_i = 0.38$), u' from the PSE has a shape close to that of a TS wave, while the one obtained from the LES does not indicate a phase inversion in the inviscid region ($y/\delta^* = 3.0$). However, there is good agreement between both far from this region. The perturbation reaches a maximum amplitude at $y/\delta^* = 1.02$, close to the boundary layer edge. Notice that the PSE indicates that this mode is stable, making the presence of a viscous instability unlikely. Further downstream at $x = 0.45$, which is already in the inflectional flow region, u' presents three peaks. A near-wall peak appears in the LES results, probably associated with the inflection point in the velocity profiles. The other two peaks are located at the boundary layer edge and $y/\delta^* = 3.0$, similar to what was observed at $x = 0.35$. However, the outer-most peak is much more pronounced at $x = 0.45$. Analogous modes were observed inside recirculating flow regions (Dovgal *et al.*, 1994). This structure is observed upstream of the LSB, with the leading edge at $x = 0.50$. This supports the claim that the inflectional instabilities upstream of separation gradually turn into shear-layer modes, such as KH ones, inside the LSB (Diwan & Ramesh, 2009). At $x = 0.55$, the double-peak structure characteristic of a KH mode is observed for u', which matches the appearance of rolls in the simulations. Nevertheless, the outer-most peak is much more pronounced in the LES results than in the PSE ones. There is a close agreement between the LES and PSE profiles of v' for all x stations.

Optimal perturbation analysis (Andersson *et al.*, 1999) was performed to gain further insight into non-modal instabilities, particularly into the growth of streaks ($\alpha = 0$ struc-

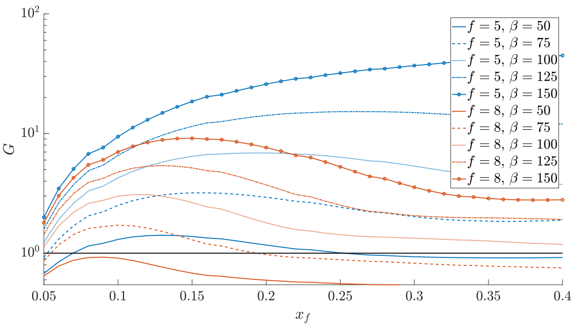

Figure 7: Growth rate of streaks as a function of the optimization location (x_f) for several spanwise wavenumbers (β) and frequencies (f).

tures) in the cases with non-zero inflow turbulence. The mean flow of the $TI = 0$ % case was employed as the basic flow for the computations. The analysis was performed for several frequencies (f), spanwise wavenumbers (β), and optimization locations (x_f), i.e., locations where the amplification reaches a maximum. The flow visualization of the $TI = 1.4$ % case (Fig. 1b) displayed streaks forming at about $x = 0.02$ and extending downstream. They initially grow quite rapidly up to around 10 % chord and then continue to grow but at a lower growth rate as was observed by following a streak moving downstream. Furthermore, from Fig. 2b and corresponding to the time instant seen in Fig. 1b, the streaks evidently possess $75 < \beta < 125$. Corresponding to this range of spanwise wavenumbers, the growth rate at different frequencies was investigated. It was found that the growth rate in the range $f = 5-8$ matches the observations from the LES. As seen in Fig. 7, at $f = 5$, a growth rate greater than $G = 1$ is seen for $\beta \geq 75$ while only β in the range of 75 to 125 follows the trajectory of a very high growth rate up to around 10 % chord followed by a reduced growth rate up to 40 % chord. At $f = 8$, this trend is observed for β between 100 and 150. A further increase in f results in streak decay ($G < 1$) for the β values obtained from the LES, at some downstream position, which was not seen in the simulation. Therefore, it can be concluded that the streaks formed at $TI = 1.4$ % with β between 75 and 125 lie within the frequency range of $f = 5$ to 8. High frequency data was not collected for the $TI = 2.8$ % case, but by comparing the PSD plots (Fig. 3), a similar frequency range experiences an increase in amplitude while the streaks from Fig. 1c seem to have a similar region of growth up to $x = 0.1$, indicating a similar range of β and f also for this case.

CONCLUSIONS

Wall-resolved large-eddy simulations of an airfoil under three turbulence intensity values are performed, and the results are analyzed in the light of linear stability analysis and optimal-perturbation theory. It is shown for $TI = 0$ % that transition is dominated by the inflectional instabilities that start to develop upstream of the LSB and gradually turn into KH modes in the separation bubble. These modes appear as rolls over the LSB, with a phase speed $c_s = 0.40$, agreeing with the values found in the literature for a KH instability, and they break down to turbulence close to the reattachment location. The $TI = 1.4$ % case presents contributions from both inflectional and streak instabilities, which are noticed by the concurrent shedding of KH rolls from the LSB and the secondary instability formed by the interaction between streaks and the LSB. These streaks possess a dimensionless frequency in the range $f = 5-8$ and a spanwise wavenumber around $\beta = 100$. Notice that their frequency is close to that of the inflectional instabilities present in the flow, making their direct interaction possible. Finally, transition in the $TI = 2.8$ % case is heavily influenced by streaks. Despite rendering the flow more stable with respect to inflectional instabilities, enhancing the near-wall momentum and reducing the LSB, these streaks are strong enough to undergo secondary instabilities, particularly of the varicose type, and thus break down to turbulence.

REFERENCES

Andersson, P., Berggren, M. & Hennignson, D. S. 1999 Optimal disturbances and bypass transition in boundary layers. *Phys. Fluids* **11** (1), 34–50.

Asai, M., Minagawa, M. & Nishioka, M. 2002 The instability and breakdown of a near-wall low-speed streak. *J. Fluid Mech.* **455**, 289–314.

Breuer, M. 2018 Effect of inflow turbulence on an airfoil flow with laminar separation bubble: An LES study. *J. Flow, Turbulence and Combustion* **101** (2), 433–456.

Burgmann, S. & Schröder, W. 2008 Investigation of the vortex induced unsteadiness of a separation bubble via time-resolved and scanning PIV measurements. *Exp. Fluids* **45**, 675–691.

Diwan, S. S. & Ramesh, O. N. 2009 On the origin of the inflectional instability of a laminar separation bubble. *J. Fluid Mech.* **629**, 263–298.

Dovgal, A. V., Kozlov, V. V. & Michalke, A. 1994 Laminar boundary layer separation: Instability and associated phenomena. *Prog. Aerosp. Sci.* **30**, 61–94.

Hain, R., Kähler, C. J. & Radespiel, R. 2009 Dynamics of laminar separation bubbles at low–Reynolds number aerofoils. *J. Fluid Mech.* **630**, 129–153.

Jones, L. E., Sandberg, R. D. & Sandham, N. D. 2010 Stability and receptivity characteristics of a laminar separation bubble on an aerofoil. *J. Fluid Mech.* **648**, 257–296.

Karp, M. & Hack, M. J. P. 2020 Optimal suppression of a separation bubble in a laminar boundary layer. *J. Fluid Mech.* **892**, 1–34.

Klein, M., Sadiki, A. & Janicka, J. 2003 A digital filter based generation of inflow data for spatially–developing direct numerical or large–eddy simulations. *J. Comput. Phys.* **186**, 652–665.

Lobo, B. A., Schaffarczyk, A. P. & Breuer, M. 2022 Investigation into boundary layer transition using wall-resolved large-eddy simulations and modeled inflow turbulence. *Wind Energy Sci.* **7** (3), 967–990.

Özçakmak, Ö. S., Madsen, H. A., Sørensen, N. N. & Sørensen, J. N. 2020 Laminar-turbulent transition characteristics of a 3-d wind turbine rotor blade based on experiments and computations. *Wind Energy Sci.* **5**, 1487–1505.

Reshotko, E. 1976 Boundary-layer stability and transition. *Ann. Rev. Fluid Mech.* **8**, 311–349.

Schaffarczyk, A. P., Schwab, D. & Breuer, M. 2017 Experimental detection of laminar–turbulent transition on a rotating wind turbine blade in the free atmosphere. *Wind Energy* **20**, 211–220.

Yarusevych, S., Kawall, J. G. & Sullivan, P. E. 2008 Separated-shear-layer development on an airfoil at low Reynolds numbers. *AIAA J.* **46**, 3060–3069.

Yuan, W., Khalid, M., Windte, J., Scholz, U. & Radespiel, R. 2005 An investigation of low–Reynolds number flows past airfoils. In *23rd AIAA Applied Aerodynamics Conference, Toronto, Ontario, Canada, June 6–9*.